Materials Today Bio 29 (2024) 101291

Contents lists available at ScienceDirect

Materials Today Bio

journal homepage: www.journals.elsevier.com/materials-today-bio

A hybrid construct with tailored 3D structure for directing pre-vascularization in engineered tissues

Sara C. Neves [a,b,c,d,#], Aureliana Sousa [a,b,#], Diana S. Nascimento [a,b,e], Iasmim D. Orge [a,e], Sílvia A. Ferreira [a], Carlos Mota [d], Lorenzo Moroni [d], Cristina C. Barrias [a,b,e,1,*], Pedro L. Granja [a,b,1,**]

[a] i3S - Instituto de Investigação e Inovação em Saúde, Universidade Do Porto, Rua Alfredo Allen, 208, 4200-135, Porto, Portugal
[b] INEB - Instituto de Engenharia Biomédica, Universidade Do Porto, Rua Alfredo Allen, 208, 4200-135, Porto, Portugal
[c] FEUP - Faculdade de Engenharia da Universidade Do Porto, Departamento de Engenharia Metalúrgica e de Materiais, Rua Dr. Roberto Frias, s/n, 4200-465, Porto, Portugal
[d] MERLN - Institute for Technology-Inspired Regenerative Medicine, Department of Complex Tissue Regeneration, Maastricht University, Universiteitssingel 40, 6229ER Maastricht, the Netherlands
[e] ICBAS - Instituto de Ciências Biomédicas Abel Salazar, Universidade Do Porto, R. de Jorge Viterbo Ferreira, 228, 4050-313, Porto, Portugal

ARTICLE INFO

Keywords:
Scaffold vascularization
Vascularized tissue
Therapeutic vascularization
Cell contact guidance
Regenerative medicine

ABSTRACT

Hybrid 3D constructs combining different structural components afford unique opportunities to engineer functional tissues. Creating functional microvascular networks within these constructs is crucial for promoting integration with host vessels and ensuring successful engraftment. Here, we present a hybrid 3D system in which poly (ethylene oxide terephthalate)/poly (butylene terephthalate) fibrous scaffolds are combined with pectin hydrogels to provide internal topography and guide the formation of microvascular beds. The sequence/method of seeding human endothelial cells (EC) and mesenchymal stromal cells (MSC) into the system had a significant impact on microvessel formation. Optimal results were obtained when EC were directly seeded onto the fibrous scaffold, followed by the addition of hydrogel-embedded MSC. This approach facilitated the development of highly oriented microvascular networks along the fibers. These networks were lumenized, supported by a basement membrane, and stabilized by pericyte-like cells, persisting for at least 28 days in vitro. Furthermore, culture under pro-angiogenic and osteoinductive conditions induced MSC osteogenic differentiation without impairing microvessel formation. Upon subcutaneous implantation in mice, the pre-vascularized constructs were infiltrated by host vessels, and human microvessels were still present after 2 weeks. Overall, the proposed hybrid 3D system, combined with an optimized cell-seeding protocol, offers an effective approach for directing the formation of robust and geometrically oriented microvessels, making it promising for tissue engineering applications.

1. Introduction

A key challenge in the fields of tissue engineering and regenerative medicine lies in accurately recreating the cellular microenvironment of human tissues. This is commonly achieved using 3D scaffolds that mimic the native extracellular matrix (ECM). These scaffolds can be designed to support and guide neo-tissue formation by replicating tissue-specific biophysical and chemical features, thereby providing optimal conditions for cell survival, proliferation, and differentiation. However, despite their satisfactory performance in vitro, cell-laden 3D constructs of clinically relevant size may ultimately fail to integrate successfully with host tissues after transplantation. The timely establishment of a perfused vascular network within these constructs is crucial, as delays can lead to insufficient oxygenation and nutrient supply, resulting in

* Corresponding author. i3S - Instituto de Investigação e Inovação em Saúde, Universidade do Porto, Rua Alfredo Allen, 208, 4200-135 Porto, Portugal.
** Corresponding author. i3S - Instituto de Investigação e Inovação em Saúde, Universidade do Porto, Rua Alfredo Allen, 208, 4200-135 Porto, Portugal.
E-mail addresses: ccbarrias@i3s.up.pt (C.C. Barrias), pgranja@i3s.up.pt (P.L. Granja).
[1] These authors contributed equally as senior authors to this work.
[#] These authors contributed equally as first authors to this work.

https://doi.org/10.1016/j.mtbio.2024.101291
Received 9 June 2024; Received in revised form 28 September 2024; Accepted 3 October 2024
Available online 4 October 2024

cellular death and tissue necrosis [1–6]. In this context, promoting in vitro pre-vascularization of engineered constructs offers a promising strategy for enhancing host-graft integration, by potentially accelerating functional vascular inosculation [1–6]. This approach typically involves seeding scaffolds with vessel-forming endothelial cells (EC), often co-cultured with stromal cells like mesenchymal stromal cells (MSC), leading to the in vitro formation of vascular networks. However, achieving sufficient microvessel maturation and stability remains a significant challenge.

Hydrogel-based matrices, which inherently mimic important features of the native ECM, are amongst the most widely used scaffolds for tissue engineering [7–9]. However, while commonly employed for cell embedding and 3D culture, traditional hydrogels often possess an isotropic nature, which can limit their capacity to direct cell behaviour. For instance, we previously showed that pectin hydrogels modified with cell-adhesive RGD peptides create an ideal 3D microenvironment for MSC organization into tissue-like multicellular networks, though these structures develop in a stochastic manner rather than following a defined pattern [9]. Moreover, hydrogels lack the necessary structural properties for repairing large, load-bearing tissue defects, which limits their overall clinical applicability.

Anisotropic hydrogel scaffolds with internal topographic features more accurately mimic the complexity and directional properties of natural tissues, offering enhanced control over the biochemical and mechanical environment experienced by cells [10,11]. Therefore, advanced chemistries and biofabrication techniques have been developed to incorporate cell contact guidance cues into hydrogels [10,11]. Strategies include layer-by-layer assembly to create anisotropic structures with varying properties across different hydrogel layers; micropatterning techniques for generating defined anisotropic features; shear-induced alignment of polymer chains and/or embedded microstructures through applied shear forces during hydrogel gelation; and the use of magnetic/electric fields to align magnetic/electrically responsive components within the hydrogel [10,11].

Alternatively, hydrogel matrices can be reinforced with fibrous structures of defined architecture and topography, providing physical guidance for cellular organization while improving structural integrity [4,12]. We have previously designed fibrous scaffolds made from poly (ethylene oxide terephthalate)/poly (butylene terephthalate) (PEOT/PBT), a biocompatible and cell-adhesive copolymer that can be easily processed through wet-spinning and additive manufacturing [13–15]. This allows precise tuning of scaffold properties such as geometry, pore size, fiber diameter, and surface topography, in contrast to traditional fabrication methods. Our earlier studies demonstrated that MSC seeded on tailored PEOT/PBT fibrous scaffolds respond to these physical properties, aligning along the fibers to form organized layers. Additionally, their differentiation potential is influenced by the scaffold's surface topography [13].

In the present study, we investigated the combination of isotropic pectin hydrogels with tailored PEOT/PBT fibrous structures as a strategy to direct microvascularization, a complex morphogenic process that requires the assembly of EC into functional tubular structures. We show that the hybrid system leverages the performance of each scaffold type, providing an optimal 3D framework for guiding the organization of co-cultured EC and MSC into stable and highly oriented microvascular beds.

Another primary objective of this study was to establish an optimal cell seeding protocol to enhance robust microvascularization in the hybrid 3D system, as prior research has demonstrated that the dynamics of endothelial and stromal cells co-seeding can significantly influence the outcome [16,17]. Therefore, different cell seeding regimens were tested by varying both the method (adding cells to the hydrogel or the fibrous scaffold) and the sequence (simultaneously or sequentially) for introducing the two cell types into the hybrid 3D system. To support its potential use in bone tissue engineering, we have also evaluated the hybrid 3D system's ability to promote both the formation of microvascular networks and the osteogenic differentiation of MSC. After optimizing the microvascularization process in vitro, we conducted a preliminary evaluation of microvessel stability after subcutaneous implantation of the pre-vascularized hybrid systems.

2. Materials and methods

2.1. Hybrid 3D system manufacturing

2.1.1. Additive manufactured PEOT/PBT fibrous scaffolds

PEOT/PBT (PolyVation B.V., Groningen, The Netherlands) fibrous scaffolds were prepared as previously described by our group [13], by combining wet-spinning with additive manufacturing (AM) to deposit polymer filaments in a spatially controlled way. The composition used in this study was 300PEOT55PBT45, consisting of PEOT and PBT in the ratio 55:45 and prepared from a starting molecular weight of PEO of 300 $g.mol^{-1}$, which presents long resorption time (> 6 months) [14]. This was considered suitable for providing long-term support for cell growth and vascular formation, without introducing confounding effects resultant from premature scaffold degradation. Briefly, PEOT/PBT was dissolved overnight (ON) at 20 % w/v in anhydrous chloroform (Sigma-Aldrich) at room temperature (RT). The solution was placed into a glass syringe fitted with a stainless-steel blunt needle (G27, inner diameter of 210 μm). A syringe pump (NE-1000, New Era Pump Systems Inc., USA) was used to control the extrusion flow rate of the polymer solution (1.5 $mL.h^{-1}$). A polytetrafluoroethylene (PTFE) tube was used to connect the syringe to a support structure placed on the plotter arm. This support structure connected the tube to the needle. A container was filled with isopropanol (Sigma-Aldrich), fixed to the fabrication platform, and used as a precipitation bath. An initial distance of 2 mm was set between the needle tip and the bottom of the container. The layer-by-layer fabrication of the scaffolds was performed using a 3D plotting machine (Envisiontec GmbH, Germany). The scaffold design used was the same as previously described [13], consisting of a 0-90° lay-down pattern, a distance between filament centers of 500 μm on both x- and y-axis and 100 μm on the z-axis. Scaffolds (cylinder-shaped, Ø 4 mm and 0.5 mm in height) were cored out from the obtained rectangular prism-like structures with a biopsy cylinder punch (Integra® Miltex®). Prior to the in vitro studies, scaffolds were incubated in 70 % v/v ethanol for 30 min, washed three times with phosphate-buffered saline (PBS), and then incubated ON at 37 °C in fibronectin (Sigma-Aldrich) solution (10 $\mu g.mL^{-1}$ in PBS) [18].

2.1.2. Peptide-modified pectin hydrogels

Pectin was purified according to an optimized protocol from the one described in the previous work by our group [9]. Briefly, a 1 % w/v solution of low methoxyl citrus pectin (Classic CU 701, degree of methylation of 37 %, containing 86 % of galacturonic acid units, kindly provided by Herbstreith & Fox, Neuenbürg, Germany) was prepared in cell culture grade endotoxin-free water (HyClone™, GE Healthcare). After the complete dissolution of the polymer, the pH of the solution was adjusted to 6 and sequentially filtered using 0.80 μm, 0.45 μm, and 0.22 μm filter membranes (mixed cellulose esters, Millipore). Activated charcoal (2 % w/v, Norit SX Plus, Norit) was added to the solution, and the suspension was stirred for 1 h at RT. The suspension was then centrifuged twice at 120000 *g* for 1 h. The supernatant was again filtered using 0.22 μm filter membranes, lyophilized, and stored at −20 °C. The purified pectin was further modified with the oligopeptide sequence $(glycine)_4$-arginine-glycine-aspartic acid-serine-proline (G_4RGDSP, Genscript, USA) by aqueous carbodiimide chemistry as previously described [9]. Pectin hydrogels (1.5 % w/v were obtained by internal gelation via ionic crosslinking using $CaCO_3$/glucono-δ-lactone (GDL)-driven gelling mechanism [9]. All pectin gels used in this study had a final RGD concentration of 150 μM, in the range of previous studies by our group [9].

2.1.3. Hybrid 3D system

Hybrid 3D systems were obtained by sequentially (i) placing the scaffolds on a PTFE plate, (ii) pipetting the cell-carrying pectin gel precursor solution over the scaffolds, and (iii) placing a second PTFE plate over the hybrid structures (with a spacing of 0.5 μm). First, the pectin gel precursor solutions were crosslinked for 1 h; after this, the cell-laden hybrid 3D systems were transferred to 24-well plates containing cell culture media. The control of the spacing between the PTFE plates was achieved using PTFE spacers of 0.5 mm. The height of the PEOT/PBT scaffolds was controlled during the additive manufacturing process, which was optimized to obtain PEOT/PBT scaffolds with a height of 0.5 mm.

2.2. In vitro studies with cell-laden 3D constructs

2.2.1. Cells sources and culture conditions

Bone marrow-derived human MSC were purchased from Lonza (PT-2501) and expanded in growth medium (MSC-GM, Lonza). Human umbilical vein endothelial cells (EC) were expanded in complete M199 medium (cM199, Sigma-Aldrich). The media of MSC and EC were changed twice and thrice a week, respectively, and cells were maintained at 37 °C under a humidified atmosphere of 5 % v/v CO_2. The detailed composition of each cell culture media used in this study is summarized in Table S1 (Supporting Information).

Different cells (between passages 5–7), material combinations, and culture conditions were used in this study (Fig. S1, Supporting Information). For the seeding of MSC and/or EC on the scaffolds, the cell number (2×10^4 cells/scaffold) was adjusted for the EC density based on Santos et al. [19]. The cell density (1×10^7 cells.mL^{-1}) used for the embedding within pectin hydrogels was in the range of the densities used in previous studies by our group [9,20]. The co-culture ratio (1:1) used for either the seeding or embedding of cells was based on previous studies on the co-culture of EC with MSC [17,21–23]. The co-culture-carrying 3D structures were cultured in endothelial culture medium (EGM-2) for 7 days and then in EGM-2:basal medium (EGM-M2: BM) or EGM-2:osteoinductive medium (EGM-2:OM) for 21 days, according to the schematics presented in Fig. S1 (Supporting Information). Control experiments (Fig. S1A) were first carried using EC, in monoculture or co-cultured with MSC, which were seeded into each type of scaffold (pectin hydrogels or PEOT/PBT scaffolds) or into the hybrid system (both cells embedded in the pectin hydrogels and added to the fibrous scaffold). Then, to test the best seeding regimen for co-cultures in the hybrid 3D system, three experimental groups were defined (Fig. S1B): (i) **EC+MSC**: EC and MSC co-embedded in pectin pre-gels and immediately added to PEOT/PBT scaffolds; (ii) **EC→MSC**: EC seeded on PEOT/PBT scaffolds, and MSC-laden pectin pre-gels added 1 week later; (iii) **MSC→EC**: MSC seeded on PEOT/PBT scaffolds, and EC-laden pectin pre-gels added 1 week later. Each in vitro experiment was repeated trice and included three replicates per tested condition.

2.2.2. Metabolic activity

Metabolic activity was estimated using a resazurin-based assay (N = 3). At different time points, the culture medium was removed from the wells, and fresh medium with resazurin (20 % v/v, Sigma) was added (400 μL per well). Next, samples were incubated (37 °C, 5 % v/v CO_2) for 2 h, after which 100 μL per well were transferred to a black 96-well plate, and the fluorescence signal was measured ($\lambda_{ex} \approx 530$ nm, $\lambda_{em} \approx 590$ nm) using a microplate reader (Synergy MX, BioTek).

2.2.3. Immunofluorescence staining and imaging

The cell-laden 3D constructs were stained for DNA, filamentous actin (F-actin) and with combinations of primary antibodies (Table S2, Supporting Information). Briefly, the cell culture medium was removed, and samples were washed with Hank's Balanced Salt Solution (HBSS, Gibco), fixed for 15–20 min in a paraformaldehyde (PFA, Electron Microscopy Sciences) solution (4 % w/v in HBSS), and permeabilized with Triton X-100 (Sigma-Aldrich) (0.1 % v/v in HBSS) for 10 min. Samples were then incubated for 1 h in a bovine serum albumin (BSA, Sigma-Aldrich) solution (1 % w/v in HBSS). Next, the 3D structures were incubated ON at 4 °C in a humidified atmosphere with BSA (1 % w/v in HBSS) with combinations of different primary antibodies (Table S2, Supporting Information). Then, samples were washed with HBSS and incubated with the BSA solution for 1 h at RT with phalloidin conjugated with Alexa Fluor® 488 (1:100, Molecular Probes®) for F-actin staining, and with the secondary antibodies goat anti-mouse Alexa Fluor® 594 and donkey anti-rabbit Alexa Fluor® 647 (1:100, Molecular Probes®). Samples were subsequently washed with HBSS solution, and DNA was counterstained with a solution of 4′,6-diamidine-2-phenylindole dihydrochloride (DAPI) (1.5 μg.mL^{-1}) in an anti-fading mounting medium (Vectashield, Vector Laboratories), 10 min before confocal microscope visualization (Leica SP5AOBS, Leica Microsystems), using LCS software (Leica Microsystems). For each sample, at least two images were obtained per each staining experiment. Representative scanned z-series of the samples were projected onto a single plane and pseudo-colored using ImageJ software [24]. Adobe Photoshop CS5® software was used for the image adjustments, namely the correction of channels levels, brightness, and contrast, and to prepare the final figure panels.

2.2.4. Analysis of the formation of microvascular structures

Confocal laser scanning microscope (CLSM, Leica SP5AOBS, Leica Microsystems) scanned z-series were projected onto a single plane, and single channels displaying CD31 and von Willebrand factor (VWF) staining were separated using ImageJ software [24]. The intensity threshold was applied after minimal background correction and manual identification and exclusion of unaligned EC staining. Results of the total area occupied by endothelial structures are expressed as a percentage of the total image area (in pixels) occupied by CD31 or VWF staining (microvessel density, measured from at least four images per condition). The diameter of the microvessels was assessed by performing several measurements per image of the length occupied by CD31 or VWF staining in the perpendicular direction of endothelial structures (at least five images per condition and at least five measurements per image). AngioTool Fiji plugin (0.6a, National Cancer Institute, USA), an open source, validated and reproducible software for quantifying vascular networks was used to calculate the Total Vessels Length in mm (at least two images per condition). Confocal images were saved as a single TIF file and converted to Imaris File Format Description (IMS) using the Imaris file converter. Converted files were read into Bitplane Imaris image visualization, segmentation and analysis software (Version 9.6.0–10.0, Oxford Instruments, Abington, UK). Surface rendering was performed for each channel containing CD31, Collagen type IV (COL IV), VWF and VE-CAD staining. A surface detail of 2 μm was chosen followed by threshold and filter settings adjusted according to image intensities and quality. After surface segmentations, video and sections of lumens were selected and ImarisVantage statistical data visualization module was used to calculate: 1) Shortest Distance of CD31 surface to nearest neighbour COL IV surface to assess the distribution of produced COL IV; and 2) Overlapped Volume ratios between VWF and VE-CAD or CD31 and COL IV surfaces to assess the proportion of dual staining in five randomly chosen vessels fragments per image with volumes ranging from 1000 to 2500 μm^3.

2.2.5. Osteogenic differentiation

Analyses of stained whole-mounted cell-laden hybrid systems were performed to identify alkaline phosphatase (ALP) activity and deposition of phosphate aggregates. First, the cell culture medium was removed, samples were washed with HBSS, and they were fixed for 15 min in the PFA solution. Next, ALP stain was performed by washing the fixed samples twice with deionized water (dH_2O) and incubating them in a Fast Violet B salt solution (0.25 mg mL^{-1} dH_2O, Sigma-Aldrich) containing 4 % v/v of naphthol AS-MX phosphate alkaline solution (0.25 % w/v, Sigma-Aldrich) for 45 min at RT, protected from light.

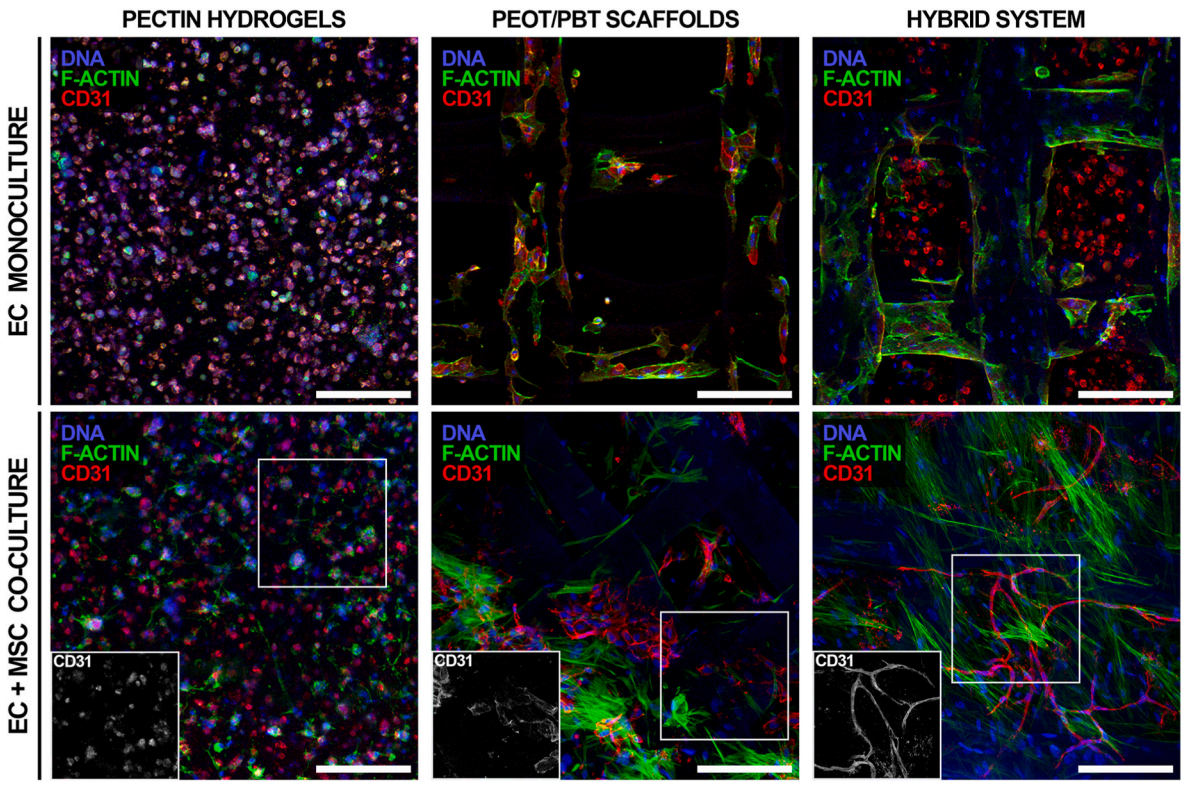

Fig. 1. The hybrid 3D system supports EC organization into microvascular networks when co-cultured with MSC. Representative confocal microscopy images of EC monoculture or EC+MSC co-culture for 28 days in pectin hydrogels, PEOT/PBT scaffolds, and 3D hybrid structures (Pseudo-colouring of DNA, F-actin, and CD31). Z-projections have a total depth of at least 100 μm. Scale bars: 200 μm.

After incubation, samples were washed twice with dH_2O. For the von Kossa (VK) stain, the previously fixed samples were washed twice with dH_2O and incubated with a silver nitrate solution (2.5 % w/v in dH_2O, Sigma-Aldrich) for 30 min under UV light at RT. Then, samples were thoroughly washed with dH_2O and incubated for 2–3 min with a sodium thiosulfate solution (5 % w/v in dH_2O, Sigma-Aldrich), after which they were again rinsed with dH_2O. Samples were imaged using a stereo microscope (Olympus SZX10) coupled with a camera (DP21 Olympus). For intensity comparison, ALP and VK stained samples were imaged with the same exposure time of 1/100 s and 1/25 s, respectively. For each sample, at least two images were obtained per staining experiment.

2.3. Preliminary in vivo studies with pre-vascularized hybrid 3D systems

2.3.1. Subcutaneous implantation in immunodeficient mice

Animal experiments were conducted following a protocol approved by the Ethics Committee of *Direção Geral de Alimentação e Veterinária* (DGAV) according to EU Directive 2010/63/EU. Severe combined immunodeficient (SCID) male mice with 6 weeks were used as recipients. Animals were housed at 22 °C with a 12 h light/dark cycle with *ad libitum* access to water and food. Analgesics (Butorfanol) were administrated 30 min prior to surgery. Animals were anesthetized by inhalation of isoflurane, which was continuously delivered throughout the surgery. The dorsal surgical sites were sterilized, and single incisions were made to create subcutaneous pockets to insert the 3D constructs. Two groups were tested: **EC+MSC** and **EC→MSC**, which were implanted after in vitro priming to induce pre-vascularization (7 days of culture after adding the cell-laden hydrogel to the fibrous scaffolds). A total of N = 6 samples were implanted per experimental group for each time point. At each endpoint (days 7 and 14), unconjugated *Griffonia simplicifolia* Lectin I (GSL I, FL-1100 Vector Labs, hereafter referred to as Lectin) was delivered via intravenous injection in the tail and 20 min after mice were euthanized by isoflurane inhalation followed by cervical dislocation. The hybrid 3D systems and surrounding tissue were collected and fixed in 4 % (w/v) PFA solution.

2.3.2. Histological and immunohistochemical (IHC) analysis

Samples were analysed as whole-mounts (N = 3) by CLSM after immunostaining and paraffin-embedded and sectioned (3 μm thick) for histochemical analysis (N = 6). For histological analysis, sections were stained with Hematoxylin Eosin and Safranin-O/Light Green (Sigma), and slides were digitalized using a scanner (NanoZoomer 2.0, Hamamatsu). The number of blood vessels (perfused with erythrocytes) detected inside the 3D hybrid scaffold was quantified using four histology sections per sample.

For immunostaining, whole-mounted samples were permeabilized with 0.25 % v/v Triton X-100, blocked with 5 % FBS; incubated (ON at 4 °C) with different antibodies (detailed information is provided on Supporting Information Table S2) for the identification of VWF, COL I and CD31 [25]. For the detection of perfused vessels, samples were incubated with goat anti-lectin antibody (Vector labs).

After that, samples were washed with PBS and incubated with the corresponding fluorochrome-conjugated secondary (Alexa-Fluor, Invitrogen) for 1 h at RT and then mounted in Vectashield™ with DAPI. Controls for each immunolabelling excluded primary antibody staining. Some samples were also stained for F-actin with phalloidin Alexa Fluor® 488 (1:100, Molecular Probes®) for 1 h at RT. Images were acquired using a Leica TCS SP5 AOBS spectral confocal microscope (Leica Microsystems, Germany and the LCS software (Leica Microsystems).

2.4. Statistical analyses

Statistical analyses were performed using GraphPad Prism 8.0 software for macOS (version 8.1.2 (227)). Data displayed in Figs. 3A and 5C regarding the metabolic activity of the different conditions (represented as mean and standard deviation) were analysed using a non-parametric

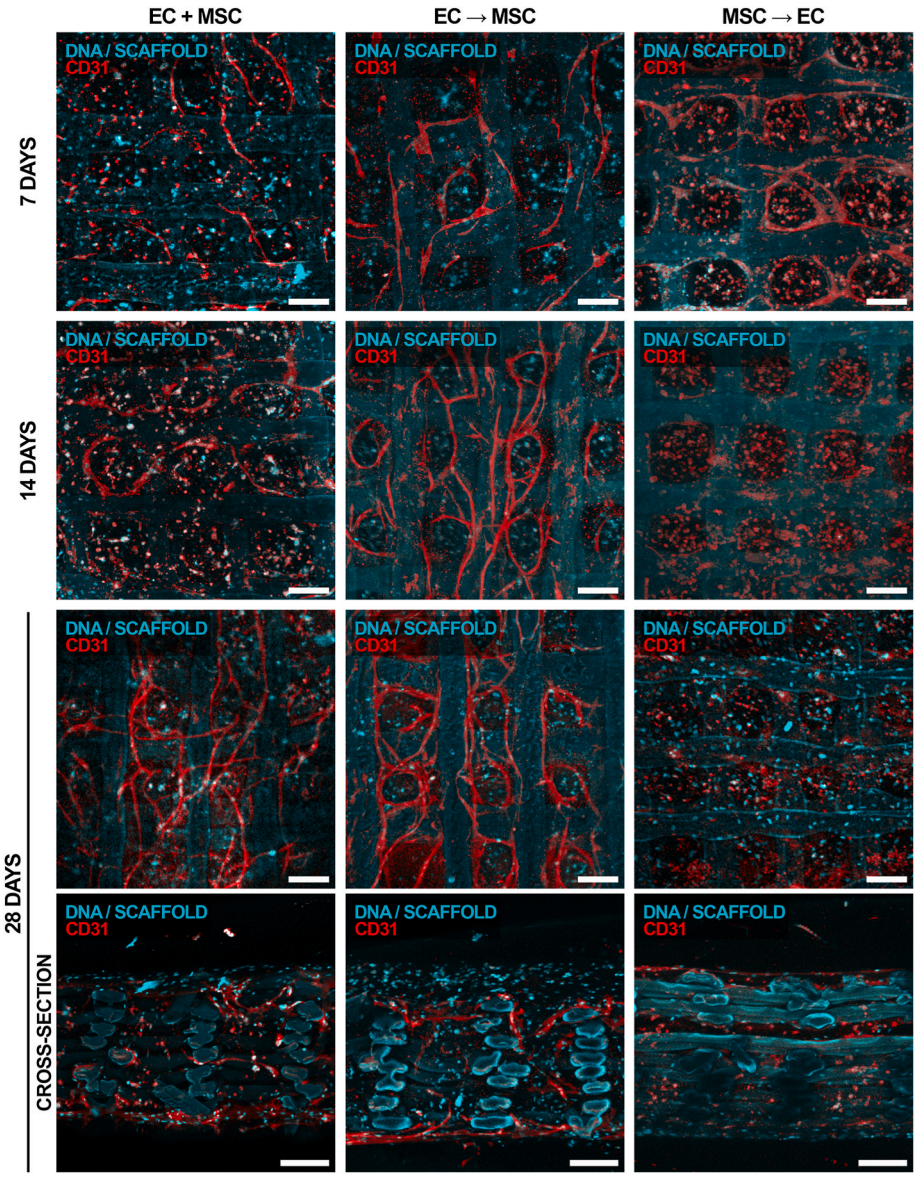

Fig. 2. The cell seeding regimen impacts the microvascularization of the hybrid 3D system. Representative confocal microscopy images of the experimental groups at 7, 14, and 28 days of co-culture (pseudo-colouring of DNA, CD31, and the scaffolds). For additional information concerning the spatial distribution of both cell types within the scaffolds, DNA, F-actin, and CD31 immunostaining images can be found in Figure S3 (Supporting Information). Z-projections have a total depth of at least 100 μm. Scale bars: 200 μm.

unpaired *t*-test with Welch's correction, with a 95 % confidence interval. Data displayed in Figs. 3A and 5C regarding the measurements of the microvessels' density assessed by CD31/VWF staining intensity (represented as the mean and standard error of the mean) was analysed using the non-parametric Mann–Whitney using a 95 % confidence interval. Data displayed in Figs. 3A and 5C regarding the measurements of the microvessels diameter (represented as the mean and standard error of the mean) was analysed using Kuskal-Wallis test with Dunn's post-test. Data displayed in Fig. 7C regarding the vessel number per scaffold section (represented as the mean and standard deviation) was analysed using the non-parametric Mann–Whitney using a 95 % confidence interval. Statistically significant differences in the different analyses are specified in the figure legend of the corresponding data.

3. Results

3.1. Endothelial organization into capillary-like structures

We first analysed the impact of culturing EC in the hybrid 3D system compared to each individual scaffold (RGD-modified pectin hydrogels or PEOT/PBT fibrous scaffolds) on their ability to form microvascular networks. EC were seeded on the different scaffolds either alone or co-cultured with MSC under the following conditions (Fig. S1A): i) cells embedded in pectin hydrogels (control); ii) cells seeded on PEOT/PBT fibrous scaffolds (control); and iii) cells embedded in a pectin pre-gel solution, which was subsequently loaded into the PEOT/PBT fibrous scaffolds for in situ crosslinking (hybrid 3D system). As depicted in Fig. 1, EC in monoculture failed to assemble into capillary-like structures in all the 3D settings, even after 28 days of culture, showing the importance of adding supportive stromal cells to the system. When in co-culture with MSC, EC also failed to organize when embedded in pectin hydrogels, where they remained essentially round, or seeded on PEOT/

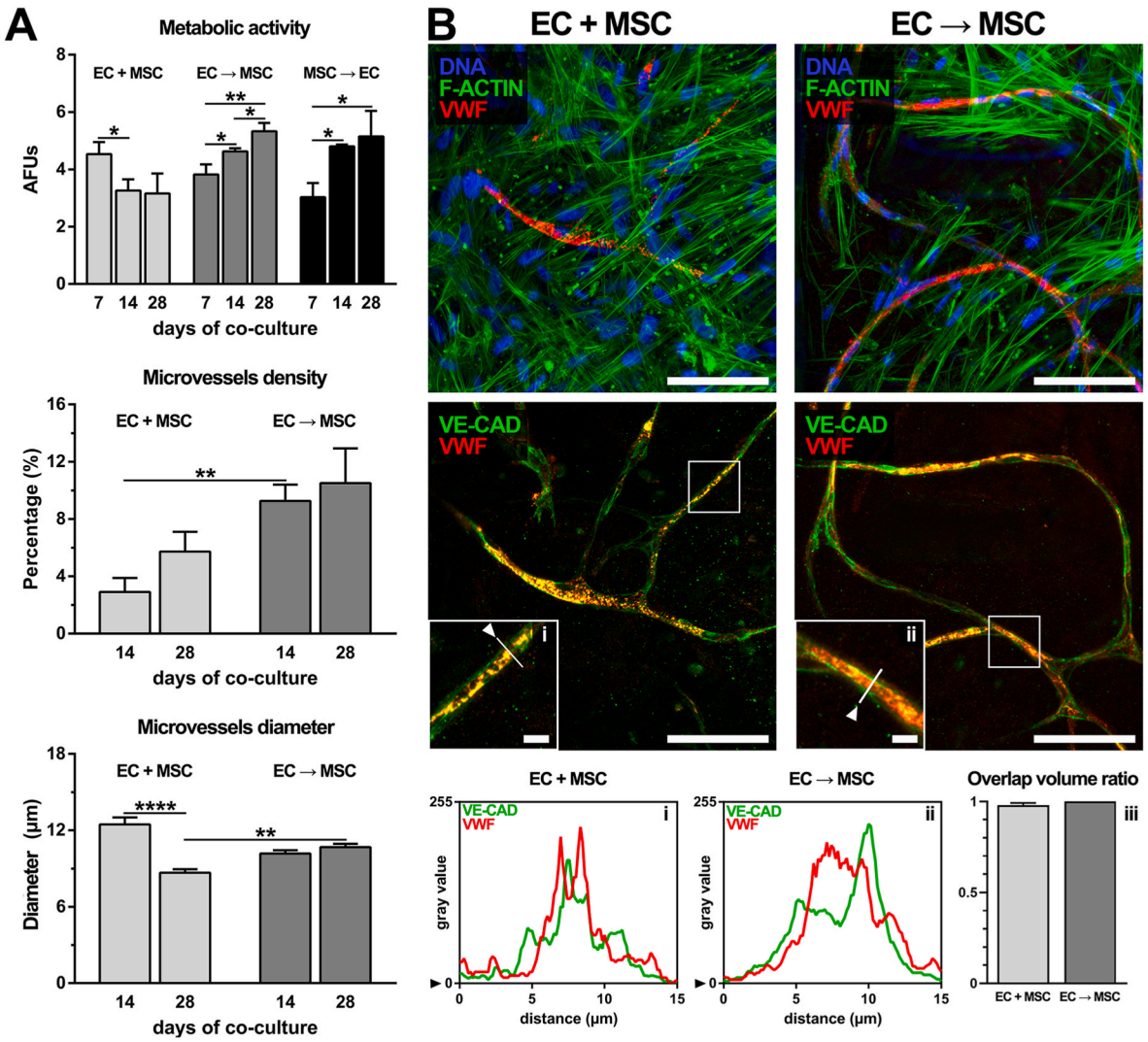

Fig. 3. The cell seeding regimen impacts the formation and stability of microvessels. (A) Metabolic activity, microvessels density, and corresponding diameter of experimental groups. Statistical significance difference identified with * ($p < 0.05$), ** ($p < 0.01$), **** ($p < 0.0001$). **(B)** Representative confocal microscopy images of the EC+MSC and EC→MSC experimental groups on day 28 of co-culture (scale bars: 100 μm). Pseudo-colouring of DNA, F-actin, and VWF (top panel), and VE-CAD and VWF (bottom panel) (scale bars of zoomed-in areas: 10 μm). Z-projections have a total depth of at least 80 μm. Graphical representation of the VE-CAD and VWF dual staining through a length of 15 μm (identified by the arrows) perpendicular to aligned EC in the zoomed-in areas (i) and (ii) and (iii) overlap volume ratio to VE-CAD with VWF-stained microvessel segments in the depicted images.

PBT fibrous scaffolds, where they formed monolayer patches at the surface. Notably, the hybrid 3D system provided an ideal 3D framework for the formation of capillary-like structures and was used in subsequent studies, where various cell seeding protocols were tested to optimize the microvascularization process.

3.2. *Effect of cell seeding regimen on microvascular networks formation*

Based on previous studies [17,23], three different cell seeding regimens were tested (Fig. S1B): i) **EC+MSC**: EC and MSC co-embedded in pectin pre-gel solution and added to PEOT/PBT scaffolds; (ii) **EC→MSC**: EC seeded on PEOT/PBT scaffolds, and MSC-laden pectin pre-gel solution added 1 week later; iii) **MSC→EC**: MSC seeded on PEOT/PBT scaffolds, and EC-laden pre-gel solution added 1 week later. Endothelial organization into capillary-like structures was evaluated, and the 3D constructs were maintained in co-culture for up to 28 days to analyse microvessel stability. By day 7, the hybrid 3D system was uniformly colonized by EC and MSC and provisional endothelial structures were detected in all experimental groups (Fig. 2 and 3 and Fig. S2). After 28 days, cells were distributed throughout the total thickness of the structure, as shown in the cross-sectional images (Fig. 2 and Fig. S3). The MSC ($CD31^{neg}$) adhered and covered the surface of the fibrous scaffolds, forming dense layers in the **MSC→EC** group (Fig. 2 and Fig. S3). They also formed multicellular 3D networks within the hydrogel-filled pores, which was more evident in the **EC→MSC** than in the **EC+MSC** group. In the **MSC→EC** group, were MSC were seeded into the fibrous scaffolds instead of loaded in the hydrogel, this only occurred between days 14 and 28 (Fig. S3). The EC ($CD31^{pos}$) displayed different behaviours across conditions (Fig. 2 and Fig. S2). In the **EC+MSC** and **EC→MSC** conditions, capillary-like structures initially formed along the fibers of the PEOT/PBT scaffold, lining the pore walls before infiltrating deeper into the scaffold. Over time, these structures became more complex and lumenized, with the total vessel length increasing from day 7 to day 28 in the **EC→MSC** group (Fig. 3A, Fig. S2, Supplementary video 1). In contrast, in the **MSC→EC** group, the provisional endothelial structures regressed over time and were no longer detected at later time points (Fig. 2 and Fig. S2).

The total cellular metabolic activity increased over time in the **MSC→EC** and **EC→MSC** groups, while it decreased from day 7 to day 14 in the **EC+MSC** group, stabilizing thereafter (Fig. 3A). This suggests that

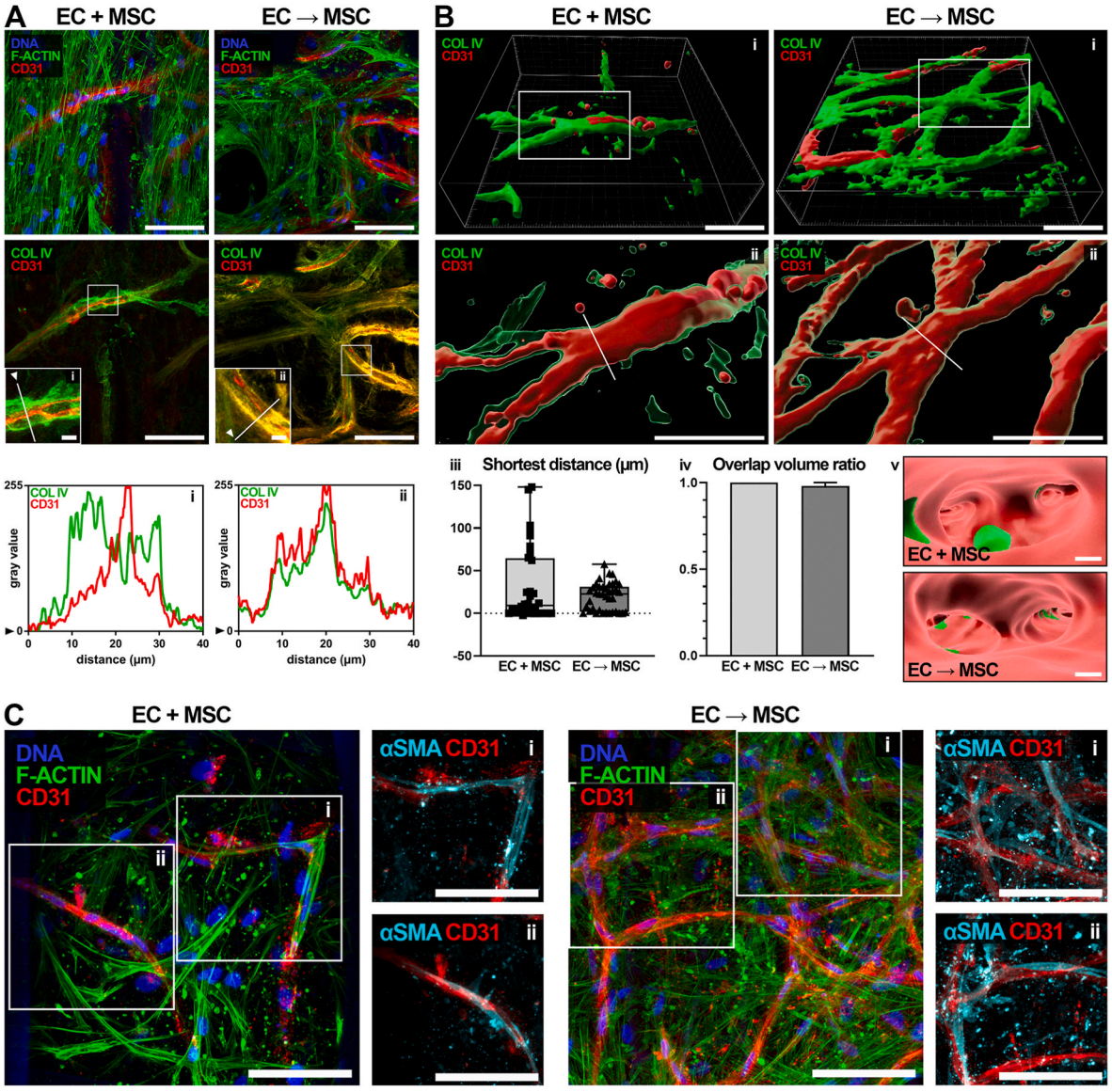

Fig. 4. Microvascular networks are stabilized by collagen type IV and perivascular cells. (A) Representative confocal microscopy images of EC+MSC and EC→MSC at 28 days of co-culture highlighting COL IV production (pseudo-colouring of DNA, F-actin, CD31, and COL IV). Graphical representation of COL IV and CD31 dual staining along a 40 μm distance (identified by the arrows) perpendicular to the microvessel in the zoomed-in areas (i) and (ii). **(B)** 3D projections of EC+MSC and EC→MSC groups at 28 days of co-culture showing the produced COL IV surrounding the microvessels' network (i) and (ii) zoomed-in areas depicting the COL IV outline, (iii) shortest distance and (iv) overlap volume ratio of produced COL IV to the microvessels in the depicted images, and (v) cross-section of the microvessel at the positions identified by the white line in (ii) showing lumens. **(C)** Representative confocal microscopy images of EC+MSC and EC→MSC at 28 days of co-culture highlighting αSMA expression (pseudo-colouring of DNA, F-actin, CD31, and αSMA). Z-projections and 3D projections have a total depth of at least 80 μm. Scale bars: 100 μm; scale bars of zoomed-in areas and insets: 10 μm).

the fibrous scaffolds offer a favourable substrate for the proliferation of cells directly seeded onto their surface [13], a process that is more restricted in hydrogel-embedded cells [9]. In the experimental groups where EC organized into stable microvessels (**EC+MSC** and **EC→MSC**), the area occupied by those structures (microvessel density) on days 14 and 28 was larger in the **EC→MSC** (9.3 ± 1.1 % and 10.5 ± 2.4 %, respectively) than in the **EC+MSC** group (2.9 ± 1.0 % and 5.7 ± 1.4 %, respectively). By day 28, the average diameters of the microvessels in both groups were comparable (ca. 9–10 μm) and in the range of human capillaries [26]. As depicted in Fig. 3B, MSC exhibited well-defined F-actin stress fibers in both groups, and EC (VWF^{pos} cells) expressed vascular endothelial cadherin (VE-CAD), which is essential for the cohesion of intercellular junctions and formation of endothelial structures [27,28]. The VE-CAD and VWF markers co-localized with nearly 100 % overlap, meaning that nearly all EC were expressing VE-CAD.

To characterize microvessel maturation, we assessed the presence of collagen type IV (COL IV), a key component of the basal lamina, and perivascular cells (αSMA^{pos}), which are crucial for capillary stabilization [29,30]. In both the **EC+MSC** and **EC→MSC** groups, COL IV expression exhibited a well-defined pattern around the CD31^{pos} tubular structures, with high degree of co-localization between the two markers, as mapped in a microvessel cross-section (Fig. 4A). Fig. 4B depicts a 3D projection of the microvascular structures, clearly showing the formation of interconnected networks, enveloped by a layer of COL IV (Fig. 4Bi and Bii). The COL IV was distributed very close to the CD31^{pos} microvessels, with a significant degree of volumetric overlap (Fig. 4Biii and Biv). Additionally, these mature microvessels were fully lumenized (Fig. 4Bv and Supplementary video 2). In contrast, the **MSC→EC** group displayed a random COL IV distribution (Fig. S4), which is consistent with microvessels regression over time. Some αSMA^{pos} cells were detected

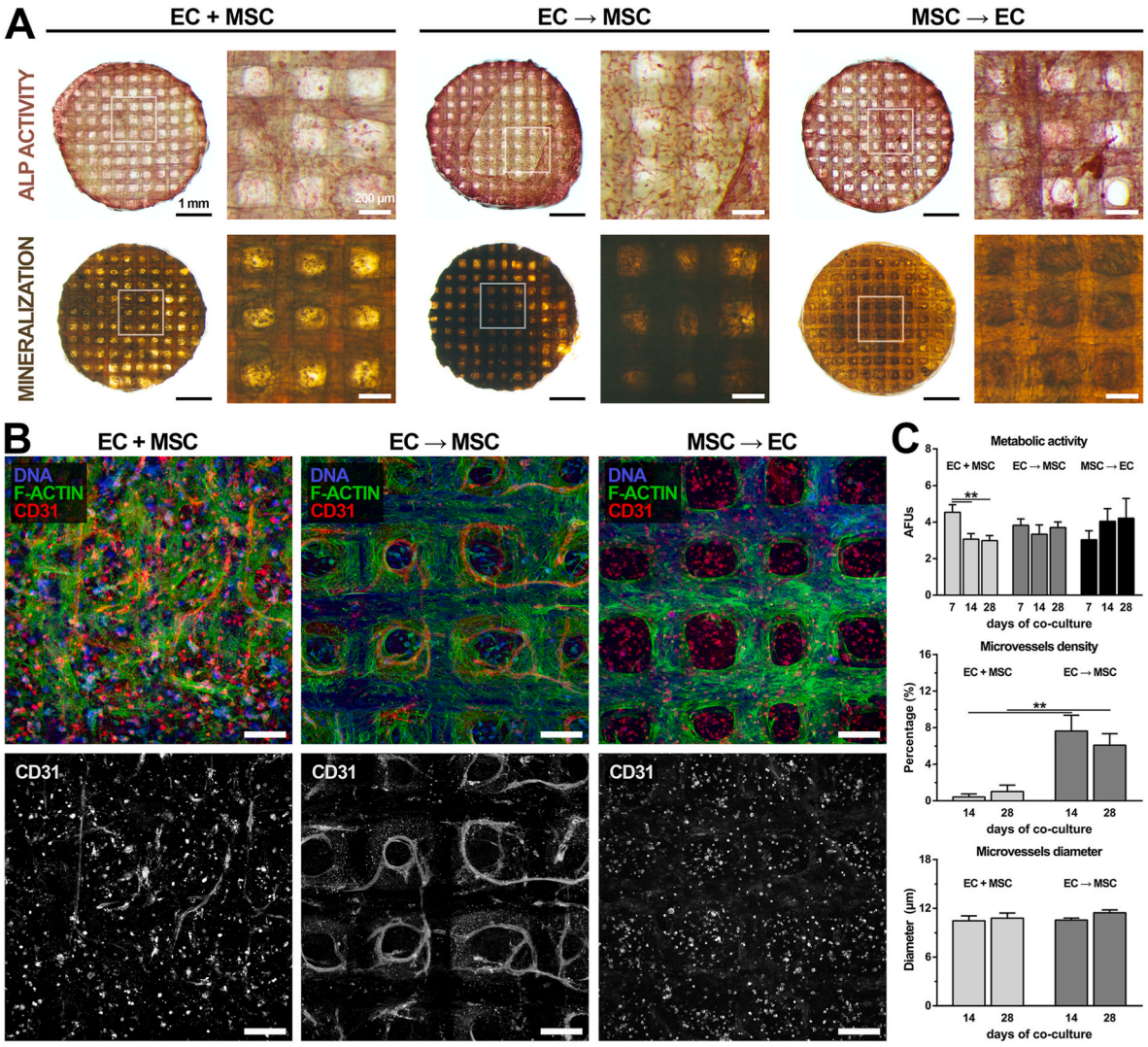

Fig. 5. The hybrid 3D system supports MSC osteogenesis and the cell seeding regimen impacts microvessel formation under osteoinductive conditions. **(A)** Representative images of the different groups after 28 days of co-culture (last 21 days in osteoinductive media) stained for ALP activity (pink stain) and mineralization (phosphate-rich compounds deposition, represented by dark brown aggregates). **(B)** Representative confocal microscopy images of the three co-culture experimental groups at 28 days of co-culture in osteoinductive media. Pseudo-colouring of DNA, F-actin, and CD31. Z-projections have a total depth of at least 100 µm. Scale bars: 200 µm. **(C)** Metabolic activity of the co-culture, microvessels density, and corresponding alignments diameters. Statistically significant differences are identified with ** ($p < 0.01$). (For interpretation of the references to colour in this figure legend, the reader is referred to the Web version of this article.)

wrapping the capillary-like structures in the **EC+MSC** and **EC→MSC** groups (Fig. 4C), but not in the **MSC→EC** group (Fig. S4). This suggest that some MSC adopted a pericyte-like phenotype, contributing to microvessel maturation and stability in the **EC+MSC** and **EC→MSC** groups.

3.3. *Microvascular network formation under osteoinductive conditions*

The 300PEOT55PBT45 formulation used herein has been extensively investigated for bone tissue engineering [13,15]. Therefore, we set out to investigate whether the hybrid 3D system could support both microvascularization and MSC osteogenic differentiation, which are concurrent processes during bone formation. First, we evaluated the ability of MSC to undergo osteogenic differentiation in pro-angiogenic medium supplemented with osteoinductive factors (EGM-2:OM), as this is not a standard osteogenic formulation. To this end, we analysed the expression of classical bone differentiation markers (COL I, ALP activity, mineralization) by qualitative histochemical analysis. After 28 days of culture and for all experimental groups, the hybrid 3D systems were filled with a COL I-rich matrix (Fig. S5), which was mineralized, as indicated by the presence of dark brown nodules (von Kossa staining), and cells were expressing high levels of ALP activity (pink) (Fig. 5A). Notably, osteogenic differentiation also occurred under basal conditions (Fig. S5), i.e., in pro-angiogenic medium without osteoinductive factors (EGM-2:BM), likely due to the presence of EC, which are known to stimulate MSC osteogenic differentiation [21].

Next, we characterized the microvascular networks that were formed inside hybrid 3D systems under osteoinductive conditions (EGM-2:OM). The **EC→MSC** group yielded the best results, with less (**EC+MSC**) or no networks (**MSC→EC**) being detected in the other groups (Fig. 5B and C, S6, S7 and S8). There were no significant differences in metabolic activity across the three experimental groups, nor any significant increase over time within each group (Fig. 5C), which is consistent with the arrest of cell growth typically observed during differentiation [21]. The microvessels density in the **EC→MSC** group was higher than in the **EC+MSC** group (Fig. 5C and Fig. S6), with values of 7.6 ± 1.7 % vs. 0.4 ± 0.3 % at day 14 and 6.1 ± 1.2 % vs. 1.0 ± 0.7 % at day 28, slightly below those observed in EGM-2 medium (Fig. 3A), although their

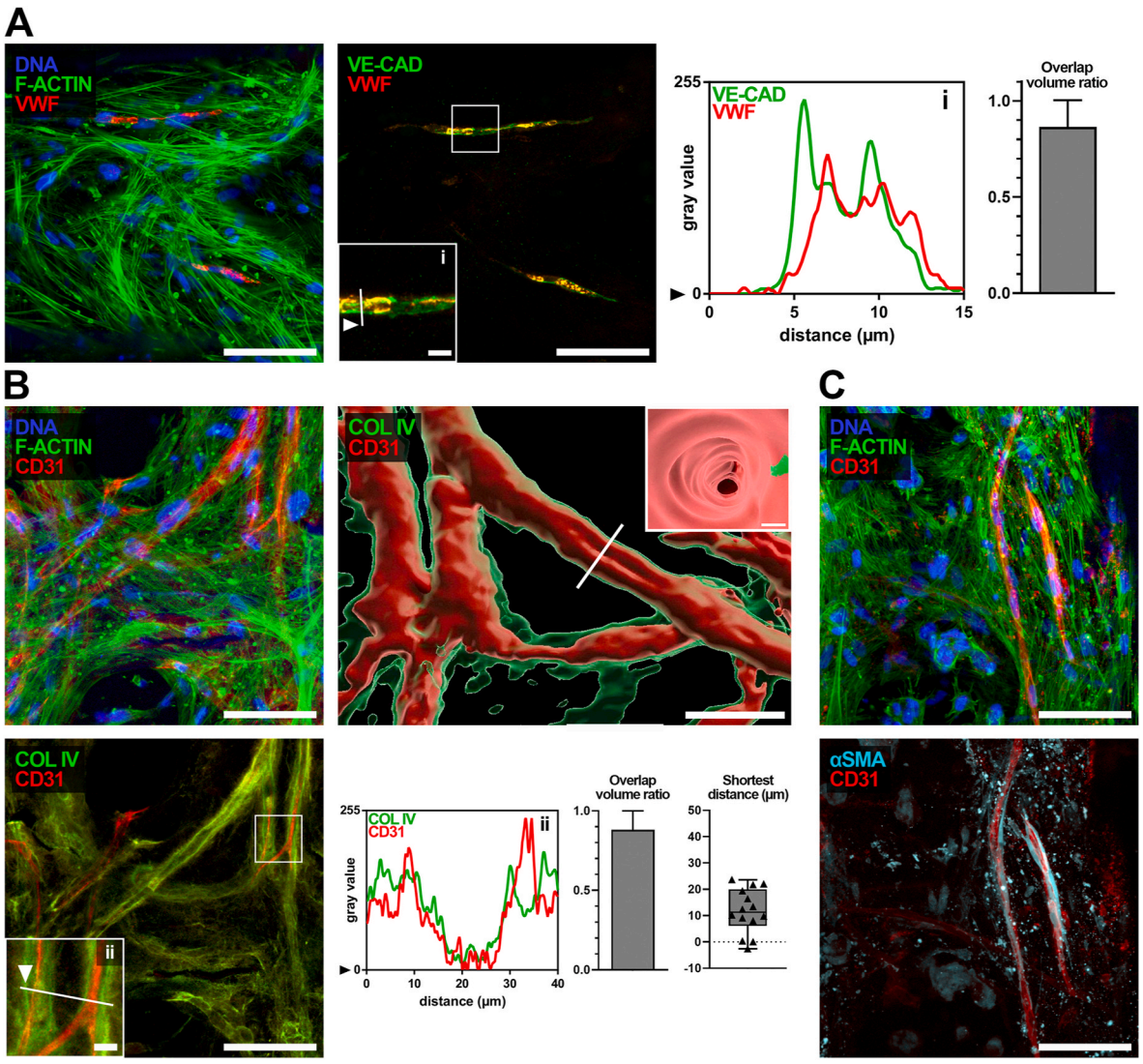

Fig. 6. EC→MSC seeding regimen shows microvascular maturation under osteoinductive conditions. Representative confocal microscopy images of the EC→MSC group at 28 days of co-culture in EGM-2:OM. **(A)** Pseudo-colouring of DNA, F-actin, and VWF (left); VE-CAD and VWF (centre); Graphical representation along a 15 μm distance (identified by the arrow) perpendicular to the microvessel of dual staining of VE-CAD and VWF from zoomed-in area (i) and overlap volume ratio to VE-CAD with VWF-stained microvessel segments in the depicted images. **(B)** Pseudo-colouring of DNA, F-actin and CD31 (top); COL IV and CD31 (bottom); Graphical representation along a 40 μm distance (identified by the arrow) perpendicular to the microvessel of dual staining COL IV and CD31 from zoomed-in area (ii). 3D projection showing the perimeter line of produced COL IV surrounding the microvessels proximity, and cross-section of the microvessel lumen at the position highlighted in white shown in the inset showing the lumen. Overlapped volume ratio and shortest distance of produced COL IV to the CD31-stained microvessels in the depicted images. **(C)** Pseudo-colouring of DNA, F-actin and CD31 (top); αSMA and CD31 (bottom). Z-projections and 3D projections have a total depth of at least 80 μm. Scale bars: 100 μm; scale bars of zoomed-in areas and inset: 10 μm).

diameters were comparable (ca. 10 μm).

Fig. 6 presents a more detailed analysis of the microvascular networks formed in the **EC→MSC** group cultured in EGM-2:OM, which presented the best outcome. Similar to that previously observed (Fig. 4A), the VWF^{pos} endothelium in microvessels expressed VE-CAD, with the two markers showing high level of overlap (Fig. 6A). The microvessels were enveloped by COL IV, indicating the presence of a basement membrane around the endothelial layer ($CD31^{pos}$) across a great extension of the network, which presented a hollow structure (Fig. 6B). Perivascular αSMA-positive cells were also detected in the vicinity of the microvessels (Fig. 6C). Overall, the **EC→MSC** group provided the most favourable condition for the in vitro formation and maturation of microvascular structures under bipotential pro-angiogenic and osteoinductive conditions.

3.4. Preliminary evaluation of the in vivo behaviour of pre-vascularized hybrid systems

Hybrid 3D systems seeded using the **EC→MSC** and **EC+MSC** approaches, both of which presented mature microvascular beds, were subcutaneously implanted in immunodeficient mice for a preliminary assessment of microvessel stability. While samples retrieved at day 7 (Fig. S9A) showed minimal blood vessel infiltration and host tissue ingrowth (Fig. S9B), constructs retrieved at day 14 were visibly vascularized and colonized by host cells (Fig. 7A). Histological analysis confirmed the infiltration of lumenized perfused vessels, filled with blood cells, within the 3D construct pores (Fig. 7B, arrow heads). This occurred at similar extent in both groups by day 14 (**EC+MSC**: 14.6 ± 5.7 and **EC→MSC**: 14.6 ± 6.2, average ± standard deviation, N = 6, Fig. 7C). The pectin hydrogel (orange staining), which was inside the pores when the construct was implanted, was partially replaced by

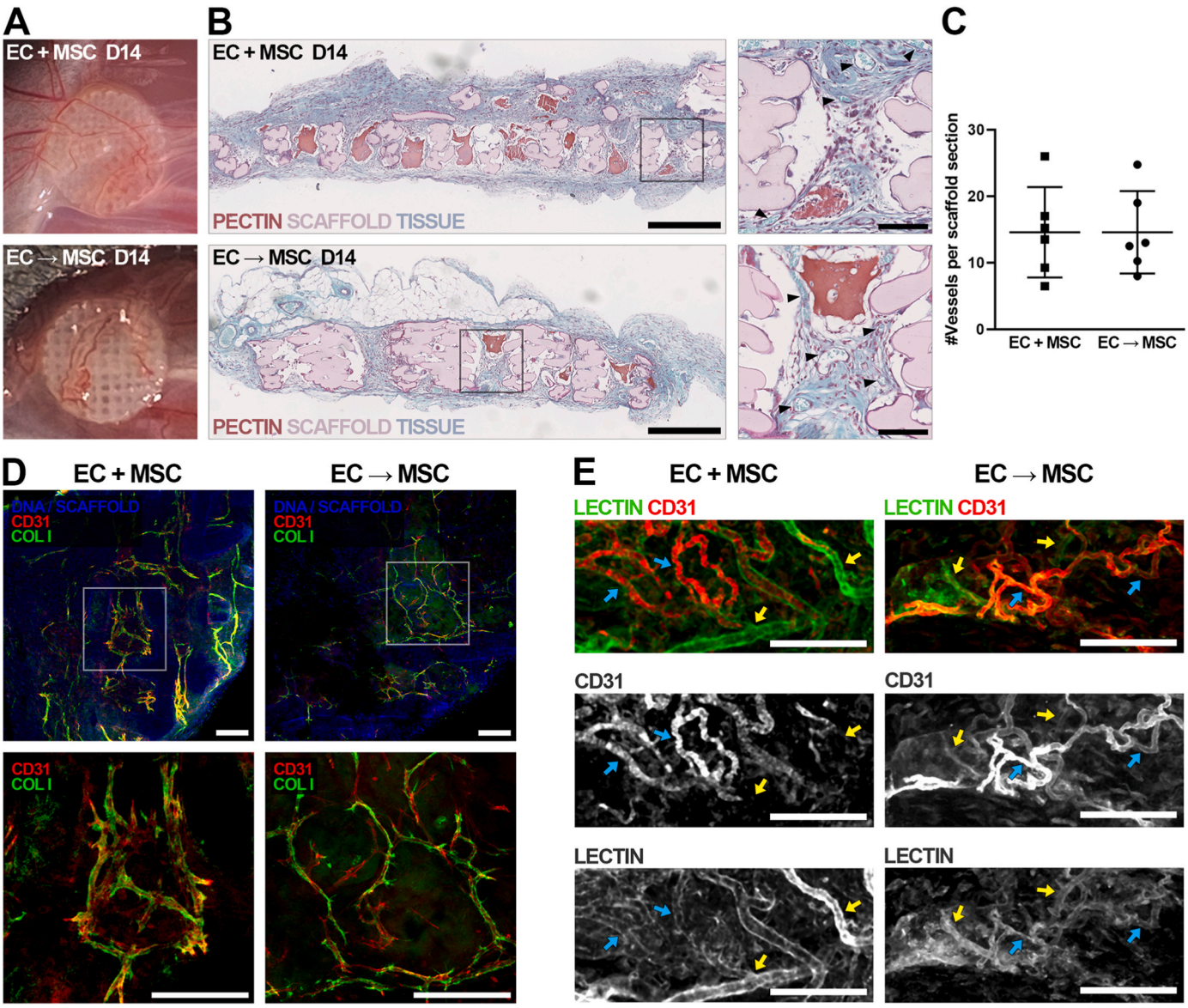

Fig. 7. Preliminary in vivo analysis of implanted pre-vascularized 3D hybrid systems. (A) Photographs of the implanted 3D hybrid structures of groups EC+MSC and EC→MSC upon retrieval (14 days of implantation). **(B)** Histological sections of the samples (groups EC+MSC and EC→MSC) retrieved after 14 days of implantation stained with Safranin-O/Light Green (scale bars: 500 μm; scale bars of zoomed-in areas: 100 μm). The arrows on the zoomed-in areas (right) identify the presence of blood cells inside lumenized microvessels. **(C)** Number of blood-perfused vessels per section of the pre-vascularized implants on day 14 (N = 6, statistically non-significant difference between groups). **(D)** Representative confocal microscopy images of EC+MSC and EC→MSC groups after 14 days of implantation. Pseudo-colouring of DNA, CD31, COL I, and scaffolds (top) and CD31 and COL I (zoomed-in area on the bottom), highlighting the presence of vascular structures (scale bars: 200 μm). **(E)** Pseudo-colouring of CD31 (red) and lectin (green) staining and the corresponding individual staining (scale bars: 100 μm). (For interpretation of the references to colour in this figure legend, the reader is referred to the Web version of this article.)

newly formed tissue (green/blue staining), as previously observed [9]. Confocal imaging of whole-mounted samples from both experimental groups revealed the presence of human microvascular networks, identified using an antibody against human CD31, within the pores of the hybrid 3D systems at day 7 (Fig. S9C). These networks persisted until day 14 (Fig. 7D). In our experimental setup, lectin was injected into the tail of each live mouse before sample retrieval to label the endothelium of perfused vessels. The lower magnification images in Fig. S10 provide an overview of the scaffolds, showing perfused vessels with larger diameters (lectin^{pos}, in green) close to smaller microvessels (CD31^{pos}, in red). The higher magnification images in Fig. 7E offer a more detailed view, showing that some microvessels, which stained strongly for anti-human CD31 (blue arrows) in contrast to other lectin^{pos} microvessels (yellow arrows), also exhibited lectin-stained endothelium. While this is a preliminary qualitative assay, it suggests that some implanted human microvessels have inosculated (i.e., connected and integrated) with the host vasculature.

4. Discussion

In this study, we used a hybrid 3D system, composed of a hydrogel structurally reinforced with a fibrous scaffold with tailored microarchitecture, to direct microvascular network formation, a critical process in tissue engineering [4–6]. For the hydrogel component, we used pectin, a versatile polysaccharide that, like alginate, undergoes ionic crosslinking under mild conditions [9]. A key difference between the two polymers is that pectin has a branched structure, rather than linear chains, resulting in the formation of 3D networks with a larger mesh size

[9]. Notably, even though the pectin backbone is not susceptible to proteolytic degradation by mammalian enzymes, the larger mesh size allows embedded MSC to mechanically remodel the matrix, facilitating cell spreading, migration, and the formation of multicellular networks [9]. This behaviour is not observed in more densely packed alginate hydrogels, where 3D cultured cells are constrained by the nanometric mesh size, remaining essentially round [7,31]. However, as shown here, pectin hydrogels do not support microvessel formation, which is a more complex and lengthy process, even when adhesive ligands are present. While the exact reasons are not fully understood, one possible explanation is that the traction forces exerted by co-cultured MSC on the matrix as they spread and interconnect lead to hydrogel contraction [9], resulting in increased matrix density. This creates a more restrictive 3D microenvironment that may hinder EC migration and organization. EC also failed to assemble into microvessels when cultured on the PEOT/PBT fibrous scaffolds, which have been widely investigated for tissue engineering applications [13–15]. Although the seeded EC were able to adhere to the surface of the fibers, they formed monolayers instead of tubular structures. This outcome is likely due to the absence of a true 3D microenvironment, which is typically provided by hydrogels.

In the hybrid system, the PEOT/PBT fibrous scaffold improved the structural integrity and mechanical support of the 3D construct, preventing excessive contraction of the pectin hydrogel. Moreover, the presence of stiffer and oriented fibers within the soft and isotropic pectin hydrogels provided physical/spatial cues for cell contact-guidance, promoting the directed migration of gel-embedded cells toward the scaffold fibers. While this hybrid configuration creates a distinct interface between areas of different stiffness and topography, rather than continuous gradients, these differences may still be sensed by the gel-embedded cells through durotaxis and/or topotaxis mechanisms [32]. Durotaxis underlies cell migration from low to high stiffness regions, where the increased strain on nascent adhesions triggers the formation of mature focal adhesion complexes that provide stronger anchorage, while topotaxis underlies cell migration along gradients of topographical features such as fibers [32]. Therefore, in our setup, the observed outcome likely resulted from a combination of these two mechanisms. To better elucidate the underlying mechanisms, future studies could focus on mapping spatial variations in mechanosensing and cytoskeletal dynamics relative to cell positioning within the hybrid system. Our observations are consistent with prior 3D studies, where EC formed geometrically oriented networks within hydrogels reinforced with fibrous scaffolds of tailored architecture, but not within the hydrogels alone [33]. With time, the deposition of cell-derived ECM along the fibers may have also contributed to modulating the development and spatial arrangement of the microvascular structures. Similarly, it was previously observed that angiogenic sprouting from EC spheroids aligns in response to ECM fibrils alignment [26].

In the hybrid system, EC were only able to self-assemble into stable vascular networks in the presence of MSC. This finding suggests that the physical cues provided by the combination of the two scaffolds synergized with the co-culture effect. Several studies have shown that supporting stromal cells, such as MSC, are critical for the formation and stabilization of nascent blood vessels [17,34–39]. In vitro, MSC have been shown to promote and support the self-assembly of EC into vessel-like networks, both indirectly through the secretion of soluble factors and ECM, and directly via cell-cell contact [35,36]. Our study confirms these previous observations. Regardless of the co-culture regimen, provisional endothelial structures in the hybrid system were formed in less than 7 days, but their maturation into stable microvascular networks was clearly dependent on the mode/sequence of addition of each cell type. The controlled incorporation of different cell types into engineered constructs, designed to replicate the temporal dynamics of tissue repair, has proven to be an effective strategy for enhancing biological outcomes [17]. However, the cell seeding protocol needs to be optimized for each new application and scaffold design [40]. For example, using a two-step protocol, Qian et al. showed that MSC seeding on an aligned ECM nanofibrous scaffold followed by EC seeding resulted in highly oriented microvessels [41]. Similarly, Krattiger et al. demonstrated that adding EC to a synthetic PEG hydrogel, decorated with cell-adhesive and protease-sensitive peptides and pre-seeded with MSC led to the formation of complex capillary networks [42]. In our system, by contrast, the **MSC→EC** set-up resulted in the formation of only a few microvessels that eventually regressed. The dense layer of MSC and their ECM covering the surface of the fibers [13], may have interfered with the hydrogel-embedded EC' ability to adhere to the scaffold and/or sense the underlying physical cues. While a direct comparison with our system is not straightforward, a previous study where EC and MSC were co-seeded in a hybrid system also showed that the accumulation of cells on the scaffold's surface hindered vascular development [16].

The most robust microvascular networks were observed in the **EC→MSC** group, where EC were initially seeded on the fibrous scaffolds, followed by the addition of gel-embedded MSC on top of the endothelialized scaffold. In this scenario, the EC adhered directly to the scaffold surface forming endothelial layers, and the hydrogel provided the necessary 3D framework for these structures to further develop into oriented microvascular networks at the fiber-hydrogel interface. This setup promoted the formation of well-organized and uniformly distributed vascular networks, with an initial morphology that followed the fibers geometry with high fidelity. This process was less efficient in the **EC+MSC**, where EC were first embedded in the hydrogel and only then added to the system. In this case, cells may have sensed the fibers' stiffness/topography, as already discussed, but they had to migrate through the hydrogel before reaching the fibers. The late addition of MSC in the **EC→MSC** compared to **EC+MSC** group may have also played a beneficial role in the microvascularization process, as previously observed. For instance, McFadden et al. [16] cultured EC alone or together with MSC, in various co-culture arrangements, by adding MSC at different stages to EC pre-seeded scaffolds. They found that the delayed addition of MSC to pre-assembled EC networks, which is similar to our **EC→MSC** group, resulted in a more robust pre-vasculature in vitro and increased in vivo vascularization potential. Using porous scaffolds of defined geometries filled with fibrin, Szklanny et al. [33], also tested different seeding protocols and showed that only the EC→SC (supportive cells) resulted in an organized vessel network. In contrast, the SC→EC and SC+EC protocols resulted in EC clustering, followed by thinning and rearranging in less developed vessels. As suggested, the delayed addition of MSC more closely mimics the natural spatio-temporal pattern of vessel formation, where EC initially assemble into provisional tubular structures that are later stabilized by the recruitment of perivascular cells [43]. One distinctive feature of our work, compared to most studies in the literature that utilize protein-derived hydrogels, is our ability to construct robust microvascular networks using pectin as the hydrogel component, which is a much less conducive polymer and lacks biological cues inherently present in those materials.

In both **EC→MSC** and **EC+MSC** groups, the presence of MSC contributed to the maturation of the neo-capillaries and prevented their regression, consistent with previous findings by others [17,34–38]. As discussed above, apart from their paracrine activity (not assessed herein), MSC also produced ECM (presence of COL I), and acted as pericytes to the nascent vessels (presence of αSMA^{pos} cells), which together promoted microvessel stabilization [30]. With time, the capillary-like structures oriented along the fibers tended to partially disengage from the scaffold, further developing throughout the hydrogel-filled scaffold pores. The diameters of the microvascular structures detected after 14 and 28 days of culture fell within the range of human microcapillaries (5–10 μm) [26].

While the ability to promote vascularization of cell-laden 3D constructs is broadly relevant for tissue engineering applications, 300PEOT55PBT45 scaffolds have been specifically investigated for bone tissue engineering due to their intermediate degradation rate and good adhesion to existing bone [14,15]. Additionally, we previously demonstrated that these scaffolds provide a suitable substrate for MSC

osteogenic differentiation [13]. Therefore, as a preliminary evaluation of the potential application of the hybrid 3D system in vascularized bone tissue engineering, we explored the feasibility of inducing microvascularization alongside MSC differentiation into osteoblasts. This is not trivial, as previous research has shown that when osteogenic media is used at the onset of the co-culture period, it may hinder the formation of EC networks [16,17]. Based on previous studies [16,17], we induced osteogenesis after inducing vascular development and confirmed that MSC were able to differentiate along the osteoblastic lineage in all groups. Interestingly, this also occurred under basal conditions (EGM-2: BM), which may possibly be explained by the well-known stimulatory effect of EC on MSC osteogenesis [44–48]. This is in line with previous research where co-cultures were established in hybrid systems [23,49], and the underlying mechanisms involved in this cellular crosstalk have been recently reviewed [50]. So, in this experimental set-up, MSC play two key roles: acting as bone progenitor cells by forming mineralized tissue and as supporting cells by stabilizing the vascular networks. Notably, culture under osteoinductive conditions – similar to those present in a bone implantation scenario – did not hinder the development of provisional endothelial structures into mature and stable microvascular beds. The best results were again obtained using the **EC→MSC** protocol, i.e., with delayed addition of MSC to the system. While further validation is needed, our results suggest that pre-vascularized hybrid 3D systems hold potential for use in bone repair applications.

We then did a preliminary assessment of microvessel stability in implanted hybrid 3D systems, which were pre-vascularized using the **EC→MSC** and **EC+MSC** protocols, as both resulted in the formation of mature microvascular networks. Previous studies have demonstrated that extending the in vitro culture of pre-vascularized 3D constructs enables the formation of more structured vascular beds, which allows for better vascular integration upon implantation [51]. Therefore, while microvessels formed within the first week of culture, the hybrid 3D systems were maintained in culture for two weeks before being subcutaneously implanted in mice for 7 and 14 days. After 14 days in vivo, the constructs demonstrated significant pro-angiogenic potential, evidenced by their ability to recruit and support the ingrowth of blood-perfused host vessels, and there were no significant differences between the two groups. This is central for successful integration with the host tissue, as it facilitates the establishment of functional connections, i.e. inosculation, between the implanted microvascular networks and the native vasculature. On the other hand, the persistence of anti-human $CD31^{pos}$ capillaries within the pores of the fibrous scaffolds after two weeks of implantation further demonstrates their stability. Furthermore, the co-localization of anti-human $CD31^{pos}$ microvessels and lectin, used here as a marker for perfused vessels, suggests that some of the implanted capillaries were able to inosculate with the host vasculature. While this was only a preliminary qualitative evaluation, and future studies are needed to accurately quantify the extent of human microvessels' integration, this finding provides an additional indicator of the implanted microvessels' stability.

5. Conclusions

The hybrid 3D system, combining RGD-modified pectin hydrogels with PEOT/PBT fibrous scaffolds guided the organization of EC, co-cultured with MSC under optimized conditions, into stable microvascular beds. The combination of the two types of scaffolds with complementary features provided an adequate physical-biochemical microenvironment for the formation of highly oriented microvessels. These presented well defined lumens and were supported by a basement membrane and pericyte-like cells, demonstrating long-term stability, both in vitro and in vivo. Additionally, the hybrid 3D system supported MSC osteogenic differentiation along with microvessels formation. Upon in vivo transplantation, the hybrid 3D system was invaded by host vessels, and the human microvessels persisted for up to two weeks. Overall, our results demonstrate the potential of pre-vascularized hybrid systems with tailored structure to serve as tissue engineering constructs with stable microvascular beds, holding promise for regenerative medicine.

CRediT authorship contribution statement

Sara C. Neves: Writing – review & editing, Writing – original draft, Visualization, Validation, Methodology, Investigation, Formal analysis, Conceptualization. **Aureliana Sousa:** Writing – review & editing, Visualization, Resources, Methodology, Investigation, Formal analysis, Conceptualization. **Diana S. Nascimento:** Writing – review & editing, Resources, Methodology, Investigation, Conceptualization. **Iasmim D. Orge:** Formal analysis, Investigation, Visualization, Writing – review & editing. **Sílvia A. Ferreira:** Formal analysis, Investigation, Visualization, Writing – review & editing. **Carlos Mota:** Validation, Resources, Investigation. **Lorenzo Moroni:** Supervision, Resources, Conceptualization. **Cristina C. Barrias:** Writing – review & editing, Writing – original draft, Visualization, Validation, Supervision, Resources, Project administration, Formal analysis, Conceptualization. **Pedro L. Granja:** Writing – original draft, Supervision, Resources, Funding acquisition, Conceptualization.

Declaration of competing interest

The authors declare that they have no known competing financial interests or personal relationships that could have appeared to influence the work reported in this paper.

Data availability

Data will be made available on request.

Acknowledgments

The authors thank the Portuguese Foundation for Science and Technology (FCT) for S. C. Neves PhD scholarship (SFRH/BD/76995/2011), I. Orge PhD scholarship (SFRH/BD/2020.07458), S. A. Ferreira contract (CEECINST/00132/2021/CP1774/CT0001). Part of this work was supported by project PTDC/BTM-ORG/5154/2020 funded by FCT. The authors acknowledge the support of i3S Scientific Platforms: "Bioimaging" member of the PPBI (Grant No: PPBI-POCI-01-0145-FEDER-022122), "Biointerfaces and Nanotechnology" (Grant No: UID/BIM/04293/2019) and "BioSciences Screening" (member of the PT-OPENSCREEN (NORTE-01-0145-FEDER-085468) and PPBI (PPBI-POCI-01-0145-FEDER-022122). The authors also acknowledge Herbstreith&Fox (Neuenbürg, Germany) for kindly providing the pectin used in this study.

Appendix A. Supplementary data

Supplementary data to this article can be found online at https://doi.org/10.1016/j.mtbio.2024.101291.

References

[1] R.E. Unger, E. Dohle, C.J. Kirkpatrick, Improving vascularization of engineered bone through the generation of pro-angiogenic effects in co-culture systems, Adv. Drug Deliv. Rev. 94 (2015) 116–125.

[2] T. Feijão, M.I. Neves, A. Sousa, A.L. Torres, S.J. Bidarra, I.D. Orge, D.T.O. Carvalho, C.C. Barrias, Engineering injectable vascularized tissues from the bottom-up: dynamics of in-gel extra-spheroid dermal tissue assembly, Biomaterials 279 (2021) 121222.

[3] I.D. Orge, H. Nogueira Pinto, M.A. Silva, S.J. Bidarra, S.A. Ferreira, I. Calejo, R. Masereeuw, S.M. Mihăilă, C.C. Barrias, Vascular units as advanced living materials for bottom-up engineering of perfusable 3D microvascular networks, Bioact. Mater. 38 (2024) 499–511.

[4] Z.-W. Tao, D.K. Jarrell, A. Robinson, E.M. Cosgriff-Hernandez, J.G. Jacot, A prevascularized polyurethane-reinforced fibrin patch improves regenerative

remodeling in a rat right ventricle replacement model, Adv. Healthc. Mater. 10 (23) (2021).
[5] A. Thibodeau, T. Galbraith, C.M. Fauvel, H.T. Khuong, F. Berthod, Repair of peripheral nerve injuries using a prevascularized cell-based tissue-engineered nerve conduit, Biomaterials 280 (2022) 121269.
[6] C. Mazio, C. Casale, G. Imparato, F. Urciuolo, C. Attanasio, M. De Gregorio, F. Rescigno, P.A. Netti, Pre-vascularized dermis model for fast and functional anastomosis with host vasculature, Biomaterials 192 (2019) 159–170.
[7] M.I. Neves, M.V. Magalhães, S.J. Bidarra, L. Moroni, C.C. Barrias, Versatile click alginate hydrogels with protease-sensitive domains as cell responsive/instructive 3D microenvironments, Carbohydr. Polym. 320 (2023) 121226.
[8] M.V. Magalhães, N. Débera, R.F. Pereira, M.I. Neves, C.C. Barrias, S.J. Bidarra, In situ crosslinkable multi-functional and cell-responsive alginate 3D matrix via thiol-maleimide click chemistry, Carbohydr. Polym. 337 (2024) 122144.
[9] S.C. Neves, D.B. Gomes, A. Sousa, S.J. Bidarra, P. Petrini, L. Moroni, C.C. Barrias, P. L. Granja, Biofunctionalized pectin hydrogels as 3D cellular microenvironments, J. Mater. Chem. B 3 (10) (2015) 2096–2108.
[10] N. Khuu, S. Kheiri, E. Kumacheva, Structurally anisotropic hydrogels for tissue engineering, Trends Chem. 3 (12) (2021) 1002–1026.
[11] S.C. Neves, L. Moroni, C.C. Barrias, P.L. Granja, Leveling up hydrogels: hybrid systems in tissue engineering, Trends Biotechnol. 38 (3) (2020) 292–315.
[12] X. Li, B. Cho, R. Martin, M. Seu, C. Zhang, Z. Zhou, J.S. Choi, X. Jiang, L. Chen, G. Walia, J. Yan, M. Callanan, H. Liu, K. Colbert, J. Morrissette-McAlmon, W. Grayson, S. Reddy, J.M. Sacks, H.-Q. Mao, Nanofiber-hydrogel composite–mediated angiogenesis for soft tissue reconstruction, Sci. Transl. Med. 11 (490) (2019) eaau6210.
[13] S.C. Neves, C. Mota, A. Longoni, C.C. Barrias, P.L. Granja, L. Moroni, Additive manufactured polymeric 3D scaffolds with tailored surface topography influence mesenchymal stromal cells activity, Biofabrication 8 (2) (2016) 025012.
[14] D. Santos, P. Wieringa, L. Moroni, X. Navarro, J.D. Valle, PEOT/PBT guides enhance nerve regeneration in long gap defects, Adv. Healthc. Mater. 6 (3) (2017) 1600298.
[15] R. Sinha, A. Sanchez, M. Camara-Torres, I.C. Uriszar-Aldaca, A.R. Calore, J. Harings, A. Gambardella, L. Ciccarelli, V. Vanzanella, M. Sisani, M. Scatto, R. Wendelbo, S. Perez, S. Villanueva, A. Matanza, A. Patelli, N. Grizzuti, C. Mota, L. Moroni, Additive manufactured scaffolds for bone tissue engineering: physical characterization of thermoplastic composites with functional fillers, ACS Appl. Polym. Mater. 3 (8) (2021) 3788–3799.
[16] T.M. McFadden, G.P. Duffy, A.B. Allen, H.Y. Stevens, S.M. Schwarzmaier, N. Plesnila, J.M. Murphy, F.P. Barry, R.E. Guldberg, F.J. O'Brien, The delayed addition of human mesenchymal stem cells to pre-formed endothelial cell networks results in functional vascularization of a collagen–glycosaminoglycan scaffold in vivo, Acta Biomater. 9 (12) (2013) 9303–9316.
[17] C. Correia, W.L. Grayson, M. Park, D. Hutton, B. Zhou, X.E. Guo, L. Niklason, R. A. Sousa, R.L. Reis, G. Vunjak-Novakovic, In vitro model of vascularized bone: synergizing vascular development and osteogenesis, PLoS One 6 (12) (2011) e28352.
[18] M.I. Santos, R.E. Unger, R.A. Sousa, R.L. Reis, C.J. Kirkpatrick, Crosstalk between osteoblasts and endothelial cells co-cultured on a polycaprolactone–starch scaffold and the in vitro development of vascularization, Biomaterials 30 (26) (2009) 4407–4415.
[19] M.I. Santos, S. Fuchs, M.E. Gomes, R.E. Unger, R.L. Reis, C.J. Kirkpatrick, Response of micro- and macrovascular endothelial cells to starch-based fiber meshes for bone tissue engineering, Biomaterials 28 (2) (2007) 240–248.
[20] S.J. Bidarra, C.C. Barrias, K.B. Fonseca, M.A. Barbosa, R.A. Soares, P.L. Granja, Injectable in situ crosslinkable RGD-modified alginate matrix for endothelial cells delivery, Biomaterials 32 (31) (2011) 7897–7904.
[21] S.J. Bidarra, C.C. Barrias, M.A. Barbosa, R. Soares, J. Amédée, P.L. Granja, Phenotypic and proliferative modulation of human mesenchymal stem cells via crosstalk with endothelial cells, Stem Cell Res. 7 (3) (2011) 186–197.
[22] H. Cui, W. Zhu, B. Holmes, L.G. Zhang, 3D Bioprinting: biologically inspired smart release system based on 3D bioprinted perfused scaffold for vascularized tissue regeneration, Adv. Sci. 3 (8) (2016).
[23] H. Cui, W. Zhu, M. Nowicki, X. Zhou, A. Khademhosseini, L.G. Zhang, Hierarchical fabrication of engineered vascularized bone biphasic constructs via dual 3D bioprinting: integrating regional bioactive factors into architectural design, Adv. Healthc. Mater. 5 (17) (2016) 2174–2181.
[24] C.A. Schneider, W.S. Rasband, K.W. Eliceiri, NIH Image to ImageJ: 25 years of image analysis, Nat. Methods 9 (7) (2012) 671–675.
[25] A.L. Torres, S.J. Bidarra, D.P. Vasconcelos, J.N. Barbosa, E.A. Silva, D. S. Nascimento, C.C. Barrias, Microvascular engineering: dynamic changes in microgel-entrapped vascular cells correlates with higher vasculogenic/angiogenic potential, Biomaterials 228 (2020) 119554.
[26] S.B. Riemenschneider, D.J. Mattia, J.S. Wendel, J.A. Schaefer, L. Ye, P.A. Guzman, R.T. Tranquillo, Inosculation and perfusion of pre-vascularized tissue patches containing aligned human microvessels after myocardial infarction, Biomaterials 97 (2016) 51–61.
[27] C. Piard, A. Jeyaram, Y. Liu, J. Caccamese, S.M. Jay, Y. Chen, J. Fisher, 3D printed HUVECs/MSCs cocultures impact cellular interactions and angiogenesis depending on cell-cell distance, Biomaterials 222 (2019), 119423-119423.
[28] D. Vestweber, VE-cadherin, arteriosclerosis, Thrombosis, and Vascular Biology 28 (2) (2008) 223–232.
[29] E. Bonanno, M. Iurlaro, J.A. Madri, R.F. Nicosia, Type IV collagen modulates angiogenesis and neovessel survival in the rat aorta model, in Vitro Cell Dev, Biol. Anim. 36 (5) (2000) 336.
[30] Z. Zhou, F. Pausch, U. Schlötzer-Schrehardt, B. Brachvogel, E. Pöschl, Induction of initial steps of angiogenic differentiation and maturation of endothelial cells by pericytes in vitro and the role of collagen IV, Histochem, Cell Biol. 145 (5) (2016) 511–525.
[31] M.I. Neves, S.J. Bidarra, M.V. Magalhães, A.L. Torres, L. Moroni, C.C. Barrias, Microstructured click hydrogels for cell contact guidance in 3D, Materials Today Bio 19 (2023) 100604.
[32] A.A. Solbu, D. Caballero, S. Damigos, S.C. Kundu, R.L. Reis, Ø. Halaas, A.S. Chahal, B.L. Strand, Assessing cell migration in hydrogels: an overview of relevant materials and methods, Materials Today Bio 18 (2023) 100537.
[33] A.A. Szklanny, L. Debbi, U. Merdler, D. Neale, A. Muñiz, B. Kaplan, S. Guo, J. Lahann, S. Levenberg, High-throughput scaffold system for studying the effect of local geometry and topology on the development and orientation of sprouting blood vessels, Adv. Funct. Mater. 30 (18) (2019).
[34] J. Ma, F. Yang, S.K. Both, H.-J. Prins, M.N. Helder, J. Pan, F.-Z. Cui, J.A. Jansen, J. J.J.P. van den Beucken, In vitro and in vivo angiogenic capacity of BM-MSCs/HUVECs and AT-MSCs/HUVECs cocultures, Biofabrication 6 (1) (2014) 015005.
[35] T.O. Pedersen, A.L. Blois, Y. Xue, Z. Xing, M. Cottler-Fox, I. Fristad, K.N. Leknes, J. B. Lorens, K. Mustafa, Osteogenic stimulatory conditions enhance growth and maturation of endothelial cell microvascular networks in culture with mesenchymal stem cells, J. Tissue Eng. 3 (1) (2012).
[36] M. Grellier, N. Ferreira-Tojais, C. Bourget, R. Bareille, F. Guillemot, J. Amédée, Role of vascular endothelial growth factor in the communication between human osteoprogenitors and endothelial cells, J. Cell. Biochem. 106 (3) (2009) 390–398.
[37] T.O. Pedersen, A.L. Blois, Y. Xue, Z. Xing, Y. Sun, A. Finne-Wistrand, J.B. Lorens, I. Fristad, K.N. Leknes, K. Mustafa, Mesenchymal stem cells induce endothelial cell quiescence and promote capillary formation, Stem Cell Res. Ther. 5 (1) (2014), 23-23.
[38] U. Blache, S. Metzger, Q. Vallmajo-Martin, I. Martin, V. Djonov, M. Ehrbar, Dual role of mesenchymal stem cells allows for microvascularized bone tissue-like environments in PEG hydrogels, Adv. Healthc. Mater. 5 (4) (2015) 489–498.
[39] P. Au, J. Tam, D. Fukumura, R.K. Jain, Bone marrow-derived mesenchymal stem cells facilitate engineering of long-lasting functional vasculature, Blood 111 (9) (2008) 4551–4558.
[40] C.T. Mierke, Physical and biological advances in endothelial cell-based engineered co-culture model systems, Semin. Cell Dev. Biol. 147 (2023) 58–69.
[41] Z. Qian, D. Sharma, W. Jia, D. Radke, T. Kamp, F. Zhao, Engineering stem cell cardiac patch with microvascular features representative of native myocardium, Theranostics 9 (8) (2019) 2143–2157.
[42] L.A. Krattiger, L.O. Moser, R. Odabasi, A. Odriozola, B.R. Simona, V. Djonov, M. W. Tibbitt, M. Ehrbar, Recovery of therapeutically ablated engineered blood-vessel networks on a plug-and-play platform, Adv. Healthc. Mater. 13 (4) (2024) 2301142.
[43] Y.J. Blinder, A. Freiman, N. Raindel, D.J. Mooney, S. Levenberg, Vasculogenic dynamics in 3D engineered tissue constructs, Sci. Rep. 5 (1) (2015) 17840.
[44] J. Kim, H.N. Kim, K.-T. Lim, Y. Kim, S. Pandey, P. Garg, Y.-H. Choung, P.-H. Choung, K.-Y. Suh, J.H. Chung, Synergistic effects of nanotopography and co-culture with endothelial cells on osteogenesis of mesenchymal stem cells, Biomaterials 34 (30) (2013) 7257–7268.
[45] Y. Kang, S. Kim, M. Fahrenholtz, A. Khademhosseini, Y. Yang, Osteogenic and angiogenic potentials of monocultured and co-cultured human-bone-marrow-derived mesenchymal stem cells and human-umbilical-vein endothelial cells on three-dimensional porous beta-tricalcium phosphate scaffold, Acta Biomater. 9 (1) (2013) 4906–4915.
[46] J.G. Gershovich, R.L. Dahlin, F.K. Kasper, A.G. Mikos, Enhanced osteogenesis in cocultures with human mesenchymal stem cells and endothelial cells on polymeric microfiber scaffolds, Tissue Eng Part A 19 (23–24) (2013) 2565–2576.
[47] M. Grellier, P.L. Granja, J.-C. Fricain, S.J. Bidarra, M. Renard, R. Bareille, C. Bourget, J. Amédée, M.A. Barbosa, The effect of the co-immobilization of human osteoprogenitors and endothelial cells within alginate microspheres on mineralization in a bone defect, Biomaterials 30 (19) (2009) 3271–3278.
[48] Z. Lin, X. Zhang, M.R. Fritch, Z. Li, B. Kuang, P.G. Alexander, T. Hao, G. Cao, S. Tan, K.K. Bruce, H. Lin, Engineering pre-vascularized bone-like tissue from human mesenchymal stem cells through simulating endochondral ossification, Biomaterials 283 (2022) 121451.
[49] R. Mishra, B.M. Roux, M. Posukonis, E. Bodamer, E.M. Brey, J.P. Fisher, D. Dean, Effect of prevascularization on in vivo vascularization of poly(propylene fumarate)/fibrin scaffolds, Biomaterials 77 (2016) 255–266.
[50] M. Bi, K. Yang, T. Yu, G. Wu, Q. Li, Cell-based mechanisms and strategies of co-culture system both in vivo and vitro for bone tissue engineering, Biomed. Pharmacother. 169 (2023) 115907.
[51] J. Koffler, K. Kaufman-Francis, Y. Shandalov, D. Egozi, D. Amiad Pavlov, A. Landesberg, S. Levenberg, Improved vascular organization enhances functional integration of engineered skeletal muscle grafts, Proc. Natl. Acad. Sci. U.S.A. 108 (36) (2011) 14789–14794.